JACS
JOURNAL OF THE AMERICAN CHEMICAL SOCIETY

ARTICLE

pubs.acs.org/JACS

A Successful Chemical Strategy To Induce Oligothiophene Self-Assembly into Fibers with Tunable Shape and Function

Francesca Di Maria,[†] Pasquale Olivelli,[†] Massimo Gazzano,[†] Alberto Zanelli,[†] Mariano Biasiucci,[‡] Giuseppe Gigli,[‡,∥] Denis Gentili,[#] Pasquale D'Angelo,[‡,§] Massimiliano Cavallini,[#] and Giovanna Barbarella*[,†]

[†]Istitute for Organic Synthesis and Photoreactivity (ISOF-CNR) and [#]Institute for Nanostructured Materials (ISMN-CNR), National Research Council, Via Gobetti 101, 40129 Bologna, Italy

[‡]NNL-CNR Nanoscience Institute c/o Dip. Fisica Ed. G. Marconi, La Sapienza University, Roma, Italy and Electronical Engineering Department, Tor Vergata University, Via del Politecnico, 00133 Rome, Italy

[∥]NNL-CNR Nanoscience Institute and Dip.Ingegneria Innovazione, Universitá del Salento, Via Arnesano, 73100 Lecce, Italy

Supporting Information

ABSTRACT: Functional supramolecular architectures for bottom-up organic nano- and microtechnology are a high priority research topic. We discovered a new recognition algorithm, resulting from the combination of thioalkyl substituents and head-to-head regiochemistry of substitution, to induce the spontaneous self-assembly of sulfur overrich octathiophenes into supramolecular crystalline fibers combining high charge mobility and intense fluorescence. The fibers were grown on various types of surfaces either as superhelices or straight rods depending on molecular structure. Helical fibers directly grown on a field effect transistor displayed efficient charge mobility and intrinsic 'memory effect'. Despite the fact that the oligomers did not have chirality centers, one type of hand-helicity was always predominant in helical fibers, due to the interplay of molecular atropisomerism and supramolecular helicity induced by terminal substituents. Finally, we found that the new sulfur overrich oligothiophenes can easily be prepared in high yields through ultrasound and microwave assistance in green conditions.

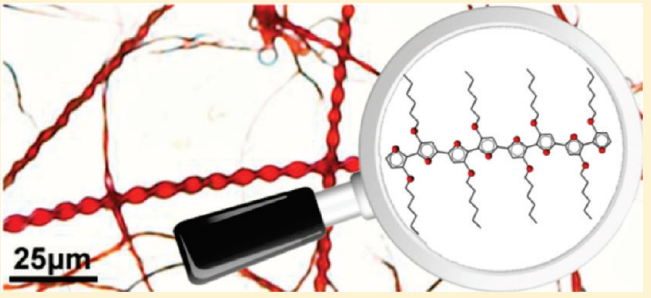

INTRODUCTION

Molecular self-assembly is a key technology for the design and bottom-up fabrication of nano- and microdevices based on soft materials. Supramolecular structures with controlled shapes, dimensions, and properties are of interest for multicomponent systems having defined function in devices for flexible electronics.[1−6] In this framework, great attention is devoted to the formation of functional nano- and microsized fibers self-organizing on surfaces which could be employed as interconnecting modules in integrated molecular circuits.[7−9]

The molecules used as building blocks for such supramolecular structures must exhibit relevant functional properties such as fluorescence, conductivity, photoconductivity, and sensitivity to external stimuli.[10] However, the molecular properties are not automatically transferred into the self-assembled superstructures, which represent novel systems from the point of view of the functional properties. Aggregation modalities and hierarchical structuring affect light emission, charge transport, and any other property in a way that is still poorly understood. No well-established rules are as yet available to relate the molecular structure to the properties of self-assembled systems, hampering the rational design of functional supramolecular architectures.

To induce diverse aggregation modalities, a variety of conjugated oligomers and polymers have been synthesized and several types of noncovalent intermolecular interactions—hydrogen bondings, van der Waals interactions, solvophobic association between aromatic rings promoting extended $\pi-\pi$ stacking—have been exploited. Results from para-hexaphenylenes bearing groups capable of multiple hydrogen bondings[11] or dyads based on alkyl substituted hexa-peri-hexabenzocoronene and perylene monoimide[12] and amphiphilic rigid macrocycles,[13] variously substituted tetrathiafulavalenes,[14] and oligoanilines[15] have been reported. Recent research has exploited the gelation properties of functional molecules to induce the formation of electroactive fibers.[16] Unfortunately, in most cases, small changes in the choice of the substrate or experimental conditions lead to distinctly different growth behavior and functional properties which are difficult to reproduce. Thus, the fibers have to be grown on the appropriate substrate and the as grown nano- and microfibers have to be manipulated and mechanically transferred for integration into a device.[17]

A crucial step forward would be the availability of molecular systems capable to reproducibly self-assemble on any type of surface. Toward this goal, we have explored new molecular design approaches and synthetic patterns to prepare oligothiophenes,

Received: February 17, 2011
Published: April 28, 2011

dx.doi.org/10.1021/ja2014949 | J. Am. Chem. Soc. 2011, 133, 8654–8661

Scheme 1. Ultrasound and Microwave Assisted Synthesis of Sulfur-Overrich Thiophene Octamers Starting from Commercial 3-Bromo-thiophene[a]

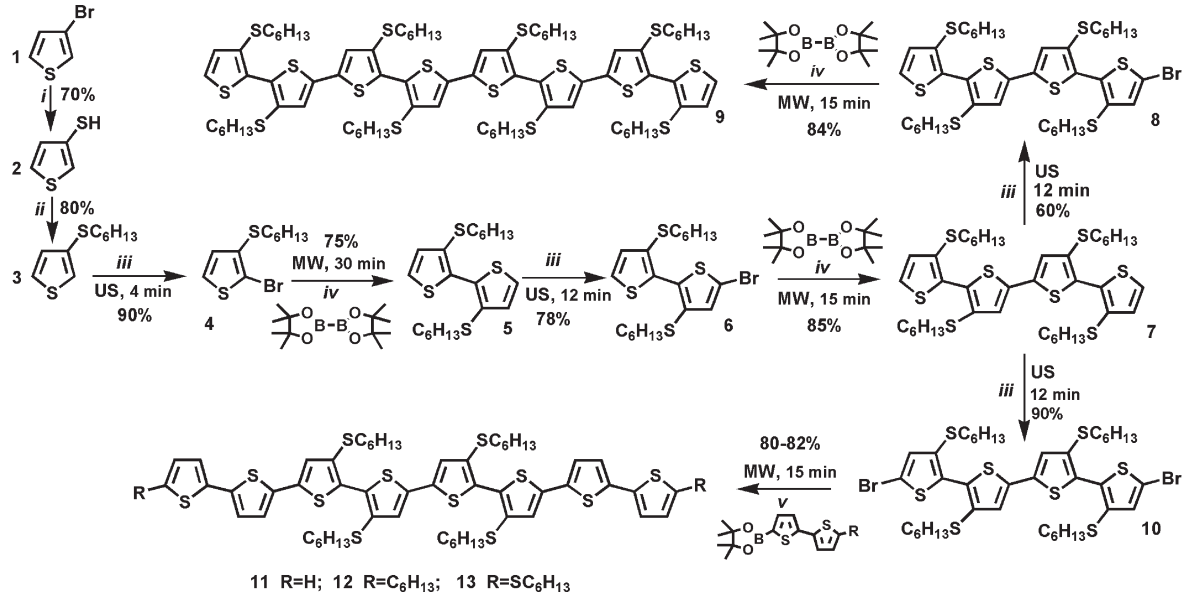

[a] (i) BuLi, S8, Et_2O; (ii) $(CH_3)3COK$, Hex-Br, EtOH; (iii) NBS (1 or 2 equiv), DMF; (iv) borolane, $NaHCO_3$, Pd(dppf)Cl_2, THF/H_2O; (v) 2-boropinacolate-2,2′-bithiophene or 2-boropinacolate,5-*S*-hexyl-2,2-bithiophene or 2-boropinacolate,5-hexyl-2,2-bithiophene, $NaHCO_3$, Pd-(dppf)Cl_2, THF/H_2O.

which are among the most efficient conjugated materials.[18,19] Owing to the great polarizability of sulfur electrons,[20−22] thiophene is an easily deformable heterocycle that in the solid state is rarely present as a regular pentagon but it is deformed, in bond angles and bond lengths, to adapt its geometry to the environment.[19] On these grounds, we chose sulfur as the key element to promote the self-assembly and created new 'sulfur-overrich' thiophene oligomers, so named since they have an extra sulfur atom per ring directly attached to one β-carbon of the inner tetrameric core, to induce ordered self-aggregation via S···S interactions and weak CH···S hydrogen bondings. On the basis of literature data,[20−23] we envisioned that the directionality of S···S and CH···S interactions, as well as the large polarizability of sulfur in thioether fragments, would induce the formation of highly anisotropic supramolecular systems.

We show here that sulfur-overrich octathiophenes do indeed self-assemble spontaneously on surfaces affording crystalline fibers combining efficient charge transport with intense fluorescence. Minor changes in the molecular structure allow the fine-tuning of fibers morphology which, although the oligomers do not bear chiral substituents, may display helical superstructure with predominance of one type of hand-helicity.

RESULTS AND DISCUSSION

A New Platform for the Synthesis of Regioregular Sulfur-Overrich Thiophene Octamers. Typically, thiophene oligomers are prepared stepwise by successive bromination and metalation of intermediates using conventional heating methods for the palladium catalyzed cross-coupling.[18,19] Here we describe a regiospecific synthesis (Scheme 1) based on Suzuki reaction[24,25] enabling the high yield synthesis of sulfur overrich regioregular thiophene octamers, rapidly prepared making use of ultrasound and microwave irradiation for the bromination and cross-coupling steps, respectively. All the octamers described in Scheme 1 are symmetric molecules characterized by an inner core made of two bithiophene subsystems bearing head-to-head β-hexylsulphanyl substituents and differing for the type of substitution at both terminal bithiophene subsystems. Efficient monobromination of mono-, di-, and quaterthiophenes was achieved in a few minutes with a single addition of NBS in DMF under ultrasound irradiation, while the formation of the dibromo derivative was negligible. In the absence of ultrasounds, the monobromination of the same substrates required the slow stepwise addition of NBS in several hours or days leading to sizable amounts of dibromo derivative.

Using commercial 4,4,5,5-tetramethyl-1,3,2-dioxa-borolane (TDB) in a one pot borylation-Suzuki coupling reaction in ethanol/water under microwave irradiation, the doubling of the oligomer skeleton was obtained in high yield and free of byproducts, thus, avoiding long and expensive purifications of the reaction products. The methodology was successfully extended to the preparation of the regioregular hexadecamer and, using the dibromobithiophene with TDB, also of the corresponding polymer (not reported).

The same methodology was also successfully used for the preparation of head-to-head oligomers and polymers bearing hexyl instead of *S*-hexyl substituents, such as octamer **6b** (Supporting Information). Thus, the combined use of ultrasound and microwave irradiation provides a very efficient platform for the rapid, low power, low cost, and environmentally friendly preparation of regioregular head-to-head thiophene oligomers and polymers.

Fibers Formation and Properties. Of the many newly synthesized sulfur overrich oligothiophenes, octamers **9** and **11**−**13** displayed the most accentuated tendency to form crystalline aggregates. The octamers achieved the right balance of size, conformation, and shape to self-assemble in ordered fibrillar structures. The formation of crystalline fibers was induced by

dx.doi.org/10.1021/ja2014949 |*J. Am. Chem. Soc.* 2011, 133, 8654–8661

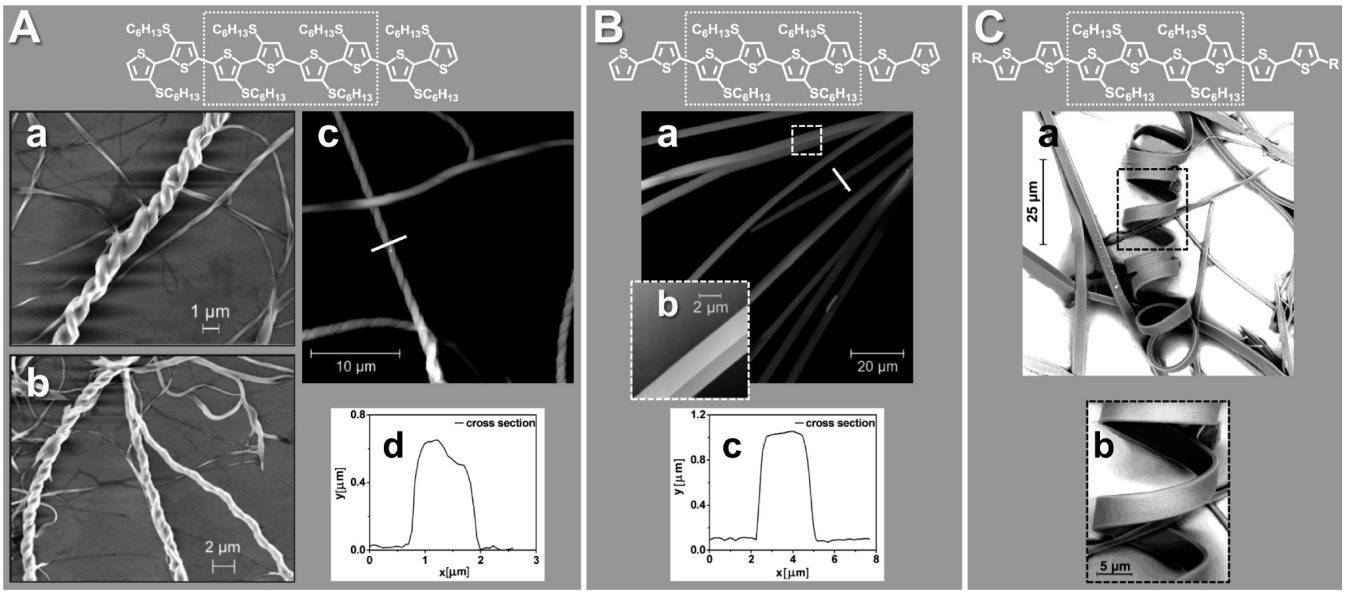

Figure 1. (A) SEM (a and b on SiO_2), AFM (c, on glass) and AFM profile (d) of fibers of **9**; (B) AFM (a, on glass) and AFM profile (b) of fibers of **11**; (C) SEM (a and b on glass) images of fibers of **12**.

dissolving at room temperature the octamers in toluene, in which they are very soluble, depositing solution drops on the surface of choice, and exposing it to vapors of acetonitrile, in which the octamers are insoluble. Randomly distributed fibers with high aspect ratio—from 1:1 to 1:2 height versus width and up to hundreds micrometers in length—were spontaneously formed (Figure 1 and Figures S7 and S8).

The directional molecular self-assembly affording fibers formation was highly reproducible, while drop casting of the octamers without exposition to acetonitrile invariably led to the formation of globular aggregates. The rate of fibers formation varied from minutes to hours, depending on concentration and molecular structure, being slower for **9** than for the other octamers. Contrary to what is generally observed with thiophene oligomers,[26,27] the shape and the formation rate of the fibers from **9** and **11**−**13** were independent of the type of surface employed: glass, ITO, silicon, and gold were employed with similar results. Generally, the aggregates formed on surfaces are the result of a balance between molecule−molecule and molecule−substrate interactions.[26,27]

Clearly, with octamers **9** and **11**−**13**, intermolecular interactions are by far more important than molecule−surface interactions and the supramolecular structures that are formed correspond to thermodynamically stable states. That the presence of the β-sulfurs plays an important role in this process is demonstrated by the fact that octamer **6b** of structure equivalent to **9** but with hexyl instead of *S*-hexyl chains (see Supporting Information) was amorphous in the experimental conditions employed for fibers formation.

Remarkably, secondary helical structure was present in most fibers with the exception of those formed by **11**, the only octamer lacking substituents on terminal bithiophene subsystems. Note that so far a 'secondary structure' has only been assigned to folded polythiophenes in solution containing chiral side chains.[18] Typically, fibers made of oligothiophenes are rod-like and strong interactions with surfaces are observed affecting film morphology.[26,27] It is generally assumed that stereocenters in the side chains are required to obtain chirality in oligothiophene fibers.[28,29] In our octamers, no chiral substituents are present and the *S*-hexyl groups promote the formation of folded or rod-like fibers depending on molecular structure, independently of the nature of the deposition surface. Octamer **9**, made of the repetition of four identical bithiophene head-to-head substituted subsystems, formed superhelices (helices of helices) and even double helices of superhelices whose periodicity was size independent (Figure 1A and Figure S6). Bigger fibrils (diameter >1 μm) were formed by several small fibrils wrapped up in themselves to form a multihelical structure, exhibiting a width versus height aspect ratio of 1:1 (Figure 1Ad) and length ranging from 100 nm to 5 μm. On the contrary, octamer **11** formed tapes-like fibrils (Figure 1Bb and Figure S6) with typical width versus height aspect ratio of 2:1 and length in the same range as **9**, which appeared atomically flat (Rms Roughness <1 nm) and with typical terraces of crystals. Finally, octamers **12** and **13**, with α,ω hexyl and *S*-hexyl chains, respectively, formed a complex network of rod-like and folded fibers terminated with astonishing ringlets (Figure 1C and Figures S7−S9). All fibers exhibited birefringence at optical polarized microscopy regardless of their specific morphology (helices vs tape-like), extinguishing in four positions at intervals of 90° by rotating the polarized light (Figure S7).

The reproducibility of morphology on different substrates upon deposition from toluene under acetonitrile vapors made possible to investigate the fibers with a variety of techniques requiring deposition on glass, ITO, SiO_2, and gold. Below we report a thorough comparative investigation on the electronic, optical, and electrical properties of the helical fibers of **9** with those, rod-like, of **11**. Circular dichroism (CD) allowed to check the chirality of the films; cyclic voltammetry (CV), the electrochemical response; confocal microscopy and space resolved spectroscopy, the light emission properties; Tunneling Atomic Force Microscopy in torsion mode (Tr-TUNA) and conductive Atomic Force Microscopy (C-AFM), the charge transport at the nanoscale. Finally, to test the applicability in devices, the fibers were directly grown on the SiO_2 surface of a field-effect transistor with gold contacts and FET charge mobilities were measured.

dx.doi.org/10.1021/ja2014949 |*J. Am. Chem. Soc.* 2011, 133, 8654–8661

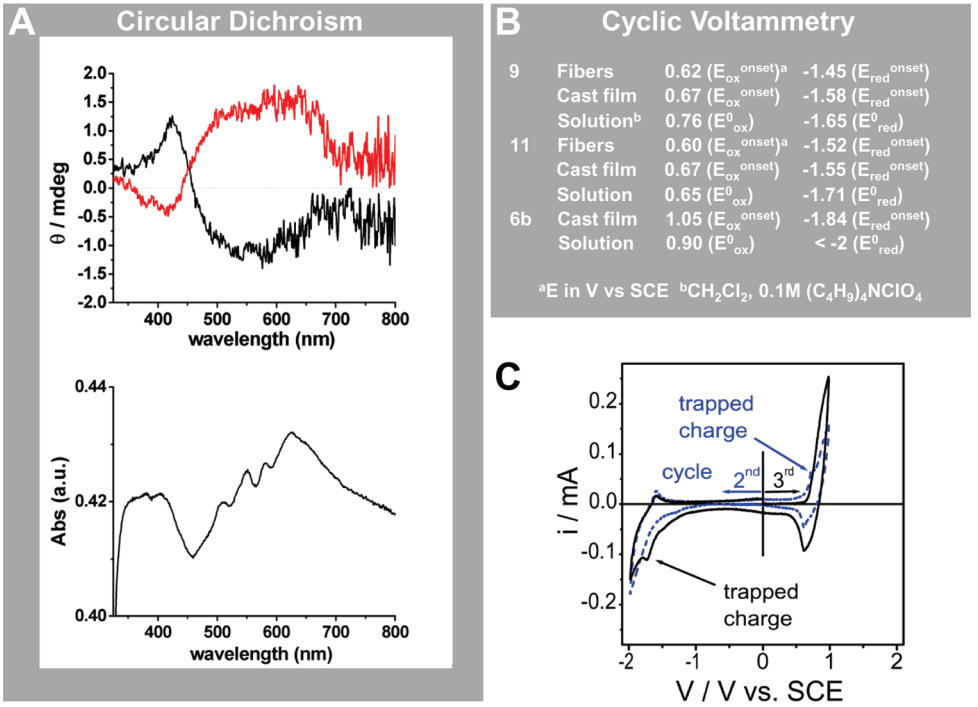

Figure 2. (A) Circular Dichroism and UV spectra of fibers of **9** formed on glass. (B) Onset potentials in PC 0.1 M $(C_2H_5)_4NBF_4$ of films of fibers and cast films (globular aggregates) of **9** and **11** on ITO, together with the redox potentials in CH_2Cl_2, 0.1 M $(C_4H_9)_4NClO_4$. For comparison, the values for **6b** (the equivalent of **9** with hexyl instead of *S*-hexyl substituents) are also reported. (C) Second and third voltammograms of the fibers film of **9** showing charge trapping phenomena.

The helical fibers formed by octamer **9** upon deposition on glass were both left- and right-handed; however, microscopy examinations suggested that one or the other type of hand-helicity was always predominating. CD measurements confirmed that the films were chiral and that the sign of chirality was random. Figure 3A displays the CD plots of two different samples of **9**, deposited on glass, that are similar but reversed in sign. Considering the thickness of the film (1−2 μm), the signal intensity is rather high. Since octamer **9** has no chiral substituents, no CD pattern was detected in solution and the chirality observed in the fibers was a property related to the supramolecular organization in the solid state. We explain the presence of the CD signal and its inversion from one sample to the other by invoking conformational atropisomerism[30,31] due to restriction of torsional processes about inter-ring C−C bonds in the solid state, which deprives the molecule of all symmetry elements rendering it chiral. Once the first molecule is frozen on the surface in the form of one or the other enantiomer (depending on the ω interring angle, $+\omega$ or $-\omega$ having equal probabilities), the conformation of the following ones is prevalently biased toward the helical sense preferred by that enantiomer causing chirality amplification.[32,33] Presumably, the handedness of the major enantiomer also affects the sign of supramolecular helicity (see Figure 5B).

Solid state electrochemistry on films of **9** and **11** deposited on ITO afforded the redox potentials shown in Figure 2B, reported as E^{onset} values.[34,35]

For comparison, also the corresponding potentials obtained for films cast from toluene (globular aggregates) and the redox potentials in solution are reported, together with the values for **6b**, the counterpart of **9** with alkyl instead of *S*-alkyl chains. The comparison of E^0 values in solution between **9** and **6b** shows the remarkable effect of side chain sulfurs on the oxidation potential, which decreases by 0.14 V, and on the reduction potential, which becomes less negative by more than 0.35 V. Going from solution to films, an analogous trend was found for both **9** and **11**. Noticeably, the helical fibers displayed the less negative reduction potential, hence the highest electron affinity. Differences in redox

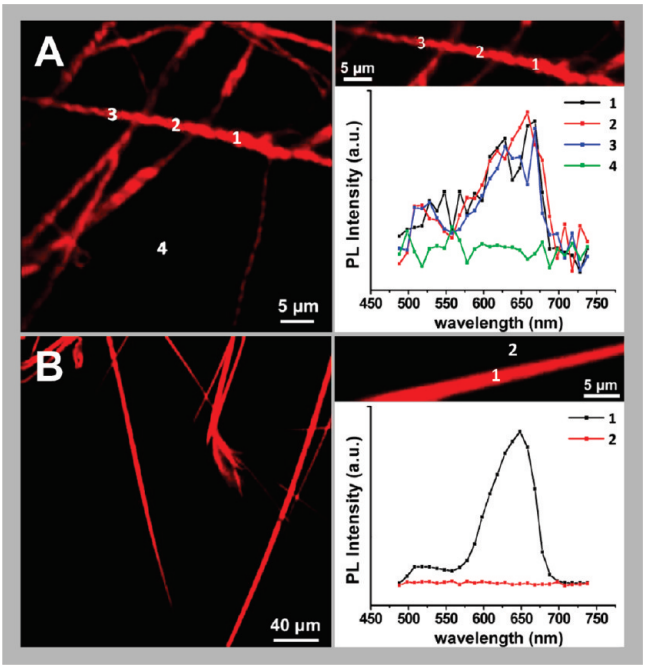

Figure 3. Laser Scanning Confocal Microscopy images and spatially resolved spectral analysis of fibers of **9** (A) and **11** (B) grown on glass.

dx.doi.org/10.1021/ja2014949 |*J. Am. Chem. Soc.* 2011, 133, 8654–8661

potentials were observed for both octamers when the morphology changed from globular aggregates to fibers, in agreement with results from literature indicating that redox potentials depend on morphology.[34,35] Interestingly, the oxidation and reduction waves of the fibers film of **9**, after the first conditioning doping, showed prepeaks (Figure 2C) indicating charge trapping phenomena similar to those observed in some polythiophenes and related to the delayed release of the charge stored during the doping process.[35,36]

All fibers were intensely fluorescent red (Figures S7,S9). Figure 3 reports laser scanning confocal microscopy (LSCM) images and spatially resolved photoluminescence (PL) spectra of fibers of **9** and **11** grown on glass.

The images, with spatial resolution of 500 nm in *x*-*y*, reveal the helical morphology of the fibers of **9** and the rod-like arrangement of the fibers of **11**. The LSCM images of **9** show spatial modulation of fluorescence along the fibers long axis. The space resolved spectra show that there is no fluorescence emission from the background and that the maximum emission wavelength of the fibers, around 650 nm for both octamers, is nearly 100 nm red-shifted with respect to the values in solution (Figure S6). The intense fluorescence observed for all fibers, including those from **12** and **13**, plaids in favor of the formation of J-type (side-by-side) rather than H-type (face-to-face) aggregates.[17] To confirm this point, detailed photophysical studies would be required which are beyond the aim of the present study. Nevertheless, the similar trend in fluorescence for all fibers suggests that their intimate molecular organization must be very similar despite differences in morphology.

Fibers of **9** and **11** grown on ITO were analyzed by Tunneling Atomic Force Microscopy in torsion mode (Tr-TUNA), a new scanning probe technique examining simultaneously surface topography and local current and providing information on nanoscale conductivity within specific domains.[37] Tr-TUNA images of fibers up to 100 μm long and with an average diameter of approximatively 300 nm are reported in Figure 4A,B. Tr-TUNA current mapping shows a direct correlation with the topography revealing defined conductive domains associated to the fibers. The variations in conductivity observed for **9** are in agreement with differences in molecules stacking within the nanodomains due to helicity, while the large, homogeneous domains associated to the fibers of **11** are in agreement with a more uniform stacking of the molecules due to the rod-like arrangement. It is worth noting that in Figure 4A the wide islands

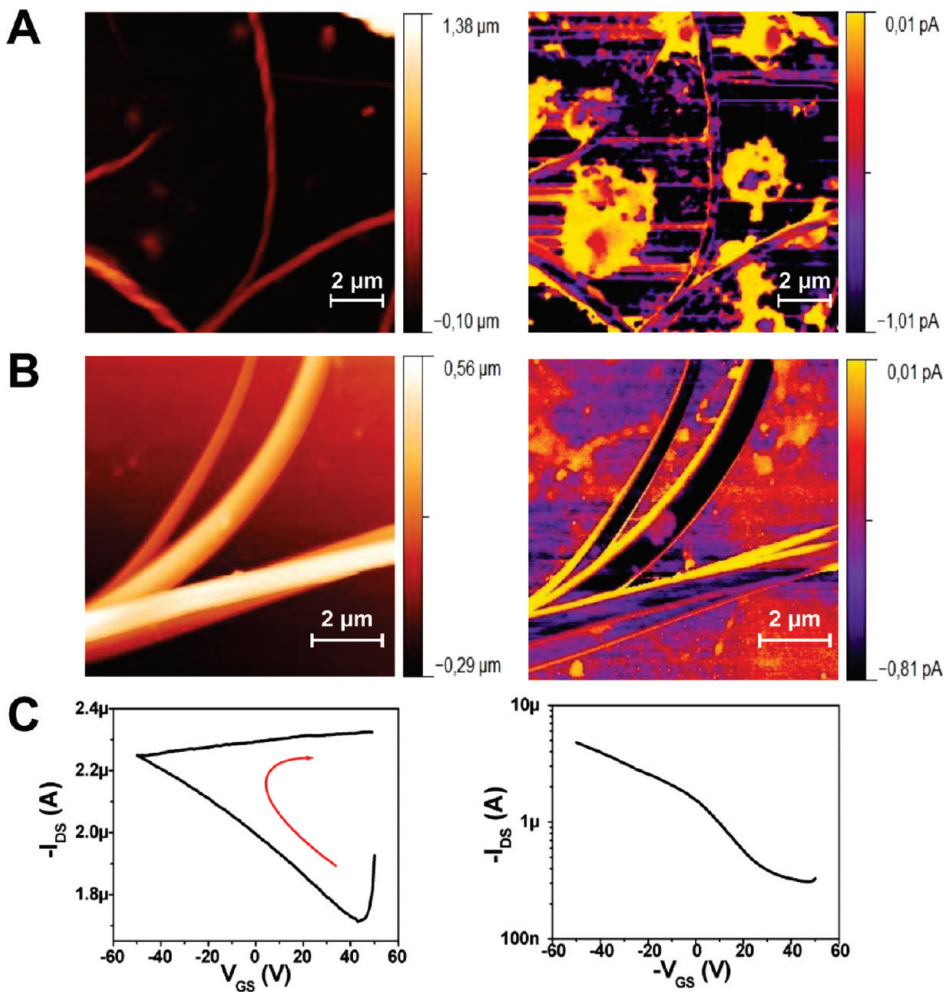

Figure 4. (A) Topography image (left) and hole transportation measurement (right) of helical fibers of **9** grown on ITO obtained using Tr-TUNA[34] with a +5 V bias on the tip. (B) The same as panel A for rod-like fibers of **11**. (C) Transfer characteristics in saturation regime in air for bottom contact field effect transistors with the active layers made of helical fibers of **9** (left) and rod-like fibers of **11** (right) directly grown on the device. The red arrow indicates the clockwise hysteresis observed on the passage from the on state to the off state, indicating an intrinsic 'memory effect' of fibers of **9**.

dx.doi.org/10.1021/ja2014949 |*J. Am. Chem. Soc.* 2011, 133, 8654–8661

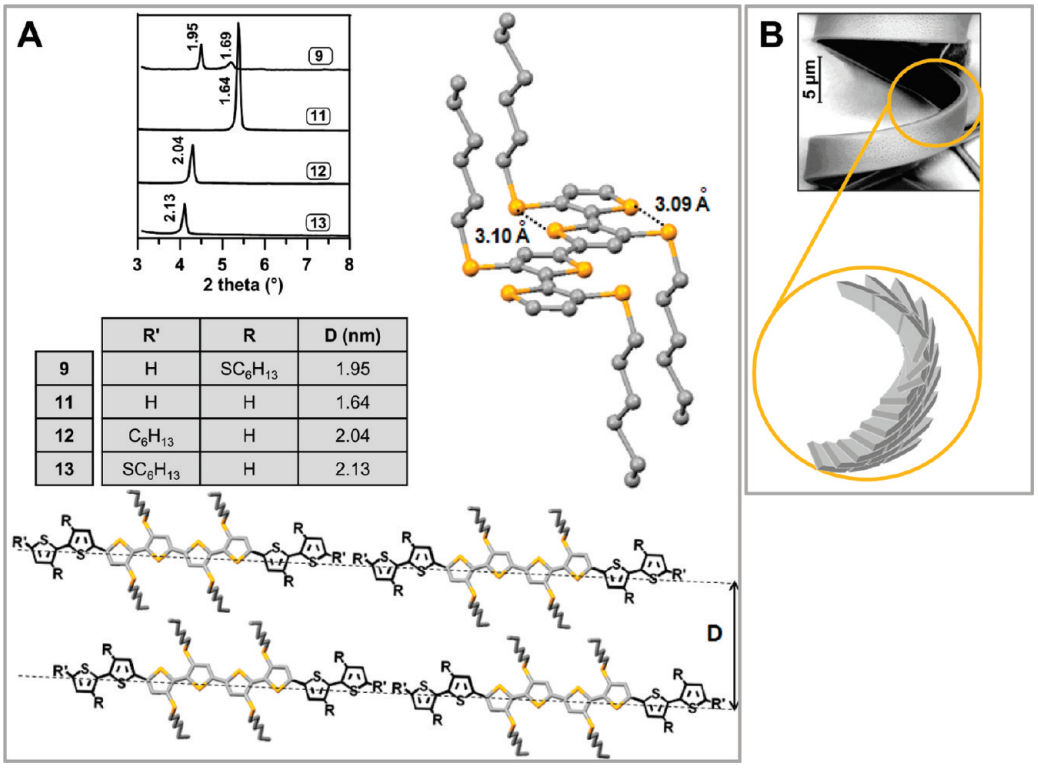

	R'	R	D (nm)
9	H	SC_6H_{13}	1.95
11	H	H	1.64
12	C_6H_{13}	H	2.04
13	SC_6H_{13}	H	2.13

Figure 5. (A) X-ray diffraction pattern of the fibers grown on glass; periodic distances reported in nm; conformation of the inner tetrameric core of the octamers as determined by single crystal X-ray analysis of **11** and model of J-type stacking. (B) A detail of the film from **12** and proposed model for the supramolecular packing.

with conductivity lower than that of the fibers have topographic correspondence in amorphous aggregates and impurities whose medium height ranges between 4 and 50 nm, much lower than the average height (300 nm) of the fibers. The islands are visible in topographic images only cutting the upper limit of the height scale suitable to make visible the topographic features of the fibers (Figures S12 and S13).

The charge (hole) mobility at the nanoscale of the fibers of **9** and **11** was obtained by measuring the charge transport trough fibers section by conductive-AFM in contact mode (C-AFM). The plots current density versus square voltage in a double logarithmic representation are reported in Figure S14. The plots showed that **9** and **11** were characterized by different charge mobility values, μ_{holes}, of 9.8×10^{-7} and 5×10^{-6} $cm^2/V \cdot s$, respectively, in agreement with Tr-TUNA maps.

Finally, since fibers morphology is independent of the substrate employed, fibers of **9** and **11** were directly grown on the SiO_2 substrate of a field effect transistor (FET) to measure the charge mobility along the fibers in the presence of an electric field. A standard two probe technique was employed to measure the drain-source current (I_{DS}) versus gate voltage (V_{GS}) for FET devices in bottom configuration (Supporting Information for details). Typical transfer characteristics in saturation regime, recorded in air, are reported in Figure 4C. Considering that, owing to the fibrillar morphology, the test patterns were effectively covered for no more than 50% of their nominal surface, μ_{holes} for **9** and **11** were 1×10^{-5} and 4×10^{-4} $cm^2\ V^{-1}\ s^{-1}$, respectively, 2 orders of magnitude higher than the intrinsic mobility measured through a single fiber in the absence of external field, and in the typical range of conductive polymers.[38] Note that FET charge mobility could be significantly improved by assembling the randomly oriented fibers into oriented functional arrays by template-directed growth. The FET based on fibres of **9** shows a peculiar feature of the material represented by the intrinsic 'memory effect,'[39] observed without recurring to polarizable gate dielectrics.[40] The 'memory effect' (Figure 4C, left, and Figure S11) is deduced from the clockwise hysteresis in drain-source current (red arrow in Figure 4C), indicating that the device retains the on state in backward gate voltage sweep, corresponding to the passage from the on to the off state. Such an effect, modulated by the gate voltage, is more pronounced in air than in vacuum and is probably related to doping from oxygen, in agreement with CV data. Remarkably, FETs based on cast films of **9** and **11** did not show any charge carrier modulation, despite the highly ordered molecular organization displayed by thin film X-ray diffraction (not reported), confirming that charge transport is strongly morphology dependent.

The consistency of the many characterization data reported above allowed us to elaborate a comprehensive model for fibers packing, as described below.

X-ray Diffraction and Fibers Packing. As shown in Figure 5A, all X-ray profiles of fibers films are dominated by the small angle reflection, other reflections being absent or of very low intensity. The distances indicated by the small angle reflection grow from 1.64 nm for **11**, without substituents on the terminal bithiophene subsystems, to 2.13 nm for **13**, having the longest terminal substituents. On the basis of these data, our hypothesis is that all octamers have a linear backbone with nearly flat conformation and, since the fibers are intensely fluorescent, the supramolecular organization is of the J-stacking type.[17] The β-thioalkyl substitution imposes anti orientation of the thiophene rings of the inner core to reduce steric hindrance and there

dx.doi.org/10.1021/ja2014949 |J. Am. Chem. Soc. 2011, 133, 8654–8661

is a parallel order of the π-conjugated cores, with the alkyl side chains extending almost perpendicularly to the thiophene backbone (Figure 5A).

In the molecular packing, the J-stacked molecules should be parallel to one another in columns at the distance obtained from the X-ray analysis (Figure 5A). We anticipate that these hypotheses are nicely confirmed by single crystal X-ray analysis of **11**, also showing that the crystalline form of this compound is the same as in powders and fibers (results to be reported in a further work). In Figure 5A, the geometry of the tetrameric inner core obtained from single crystal X-ray analysis of **11** is reported. The geometry is planar with the sulfur atoms on the same plane and S···S intermolecular distances largely below the sum of van der Waals radii (3.60 Å).

The presence of substituents in the outermost rings induces disorder effects and distorsions at the end points of the molecules that influence the distance between parallel octathiophene rows, making it vary with molecular structure. Thus, we can describe the supramolecular assembly as lamella-type structure in which the small distortions of the molecular apexes cause a slight disruption of the compact packing of the molecules simply by means of a slightly twist of long molecular axes in the short-range. The morphology is influenced by the packing order of the molecules and in the long-range ordered helixes and curls appear as macroscopic effects of stacking faults during the growth (Figure 5B).

CONCLUSIONS

In summary, we discovered a new recognition algorithm—Lenh's expression indicating the molecular features driving self-assembly via noncovalent interactions[41]—that causes the spontaneous self-assembly of octathiophenes into nano- and micrometer sized multifunctional fibers on surfaces. The new recognition algorithm resulted from the combination of thioalkyl substituents and head-to-head regiochemistry of substitution, inducing aggregation of sulfur overrich octathiophenes mainly via S···S noncovalent interactions. It led to the formation of crystalline superhelices (helices of helices), electroactive and fluorescent, in which one type of hand-helicity was always predominating despite of the absence of chiral substituents in the molecular skeleton. Contrary to what has been observed so far, fibers morphology was univocally determined by the molecular structure and reproducibly generated on various types of surfaces. Fibers directly grown on the SiO_2 substrate of a field-effect transistor displayed efficient charge conduction, indicating their usefulness for application in organic devices.

Taking advantage of X-ray diffraction data, we elaborated a comprehensive model accounting for all the observed properties and interpreting the chirality features on the basis of the interplay of molecular atropisomerism and supramolecular helicity induced by terminal substituents.

Finally, we developed, on one side, a new platform for the rapid and high yield synthesis of the materials in aqueous solvents making use of ultrasound and microwave irradiation and, on the other, a new method for fiber formation based on the action of a solvent and a nonsolvent to favor crystallization.

For all these aspects, our work represents an important progress in programming and engineering organic functional materials. Because of their crystallinity, charge transport, and fluorescence and due to the control of morphology, hence, of the functional properties, the fibers described here are suited for application in molecular based devices for organic electronics, photovoltaics, and sensing.

ASSOCIATED CONTENT

Supporting Information. Full experimental details for the synthesis of the new compounds and their precursors; H-1 and C-13 NMR spectra of octamers **9** and **11**−**13** and **6b**; optical microscopy images of octamers **9** and **11**−**13** and SEM of **13**; cyclic voltammetry data; conductive AFM; Field Effect Transistors. This material is available free of charge via the Internet at http://pubs.acs.org.

AUTHOR INFORMATION

Corresponding Author
barbarella@isof.cnr.it

Present Addresses
[§]Univ. London Imperial Coll. Sci. Technol.; Med., Dept. Chem., London SW7 2AZ, England.

ACKNOWLEDGMENT

This research was supported by projects FIRB RBPR05JH2P_ITALNANONET (G.G.), FIRB RBIP0642YL-LUCI (G.B.) and ESF-EURYI DYMOT (M.C. and D.G.).

REFERENCES

(1) Whitesides, G. M.; Grzybowski, B. *Science* **2002**, *295*, 2418–2421.
(2) Palmer, L. C.; Stupp, S. I. *Acc. Chem. Res.* **2008**, *41*, 1674–1684.
(3) Schiek, M.; Balzer, F.; Al-Shamery, K.; Brewer, J. R.; Lützen, A.; Rubahn, H.-G. *Small* **2008**, *4*, 176–181.
(4) Smits, E. C. P.; Mathijssen, S. G. J.; Van Hal, P. A.; Setayesh, S.; Geuns, T. C. T.; Mutsaers, K. A. H. A.; Cantatore, E.; Wondergem, H. J.; Werzer, O.; Resel, R.; Kemerink, M.; Kirchmeyer, S.; Muzafarov, A. M.; Ponomarenko, S. A.; De Boer, B.; Blom, P. W. M.; Leeuw, D. M. *Nature* **2008**, *455*, 956–959.
(5) Park, S.; Hamad-Schifferli, K. *Curr. Opin. Chem. Biol.* **2010**, *14*, 616–622.
(6) Yun, Y. H.; Eteshola, E.; Bhattacharya, A.; Dong, Z.; Shim, G.-S.; Conforti, L.; Kim, D.; Schulz, M. J.; Ahn, C. H.; Watts, N. *Sensors* **2009**, *9*, 9275–9299.
(7) Hasegawa, M.; Iyoda, M. *Chem. Soc. Rev.* **2010**, *39*, 2420–2427.
(8) Feng, X.; Pisula, W.; Kudernac, T.; Wu, D.; Zhi, L.; De Feyter, S.; Müllen, K. *J. Am. Chem. Soc.* **2009**, *131*, 4439–4448.
(9) Wang, Y.; Tran, H. D.; Liao, L.; Duan, X.; Kaner, R. B. *J. Am. Chem. Soc.* **2010**, *132*, 10365–10373.
(10) Whitesides, G. M.; Lipomi, D. J. *Faraday Discuss.* **2009**, *143*, 373–384.
(11) Durkut, M.; Mas-Torrent, M.; Hadley, P.; Jonkheijm, P.; Schenning, A. P. H. J.; Meijer, E. W.; George, S.; Ajayaghosh, A. *J. Chem. Phys.* **2006**, *124*, 154704/1–6.
(12) Mativetsky, J. M.; Kastler, M.; Savage, R. C.; Gentilini, D.; Palma, M.; Pisula, W.; Müllen, K.; Samor, P. *Adv. Funct. Mater.* **2009**, *19*, 2486–2494.
(13) Kim, J. K.; Lee, E.; Kim, M. C.; Sim, E.; Lee, M. *J. Am. Chem. Soc.* **2009**, *131*, 17768–17770.
(14) Tanaka, K.; Kunita, T.; Ishiguro, F.; Naka, K.; Chujo, Y. *Langmuir* **2009**, *25*, 6929–6933.
(15) Wang, Y.; Tran, H. D.; Liao, L.; Duan, X.; Kaner, R. B. *J. Am. Chem. Soc.* **2010**, *132*, 10365–10373.
(16) Prasanthkumar, S.; Saeki, A.; Seki, S.; Ajayaghosh, A. *J. Am. Chem. Soc.* **2010**, *132*, 8866–8867.

(17) An, B. K.; Gihm, S. H.; Chung, J. W.; Park, C. R.; Kwon, S. K.; Park, S. Y. *J. Am. Chem. Soc.* **2009**, *131*, 3950–3957.
(18) *Handbook of Thiophene-Based Materials*; Perepichka, I. E., Perepichka, D. F., Eds.;John Wiley & Sons: Chichester, 2009.
(19) Barbarella, G.; Melucci, M.; Sotgiu, G. *Adv. Mater.* **2005**, *17*, 1581–1593.
(20) Bernardi, F.; Csizmadia, I. G.; Mangini, A.; Schlegel, H. B.; Whangbo, M. H.; Wolfe, S. *J. Am. Chem. Soc.* **1975**, *97*, 2209–2218.
(21) Desiraju, G. R. ; Steiner, T. *The Weak Hydrogen Bond*; Oxford University Press: Oxford, 1999.
(22) Gellman, S. H. *Biochemistry* **1991**, *30*, 6633–6636.
(23) Crivillers, N.; Mass-Torrent, M.; Bromley, S. T.; Wurst, K.; Veciana, J.; Rovira, C. *ChemPhysChem* **2007**, *8*, 1565–1571.
(24) Suzuki, A. *Chem. Commun.* **2005**, 4759–4763.
(25) Alesi, S.; Di Maria, F.; Melucci, M.; Macquarrie, D. J.; Luque, R.; Barbarella, G. *Green Chem.* **2008**, *10*, 517–523.
(26) Surin, M.; Leclére, P.; De Feyter, S.; Abdel-Mottaleb, M. M. S.; De Schrywer, F. C.; Henze, O.; Feast, W. J.; Lazzaroni, R. *J. Phys. Chem. B* **2006**, *110*, 7898–7908.
(27) Balzer, F.; Schiek, M.; Lützen, A.; Rubahn, H. G. *Chem. Mater.* **2009**, *21*, 4759–4767.
(28) Leclère, P.; Surin, M.; Lazzaroni, R.; Kilbinger, A. F. M.; Henze, O.; Jonkheijm, P.; Biscarini, F.; Cavallini, M.; Feast, W. J.; Meijer, E. W.; Schenning, A. P. H. J. *J. Mater. Chem.* **2004**, *14*, 1959–1963.
(29) Henze, O.; Feast, W. J.; Gardebien, F.; Jonkheijm, P.; Lazzaroni, R.; Leclére, P.; Meijer, E. W.; Schenning, A. P. H. J. *J. Am. Chem. Soc.* **2006**, *128*, 5923–5929.
(30) Allinger, N. L.; Eliel, E. L.; Wilen, S. H. *Top. Stereochem.* **1983**, *14*, 1–81.
(31) Williams, P. L.; Giralt, E. *Chem. Soc. Rev.* **2001**, *30*, 145–157.
(32) Van Gestel, J. *J. Phys. Chem. B* **2006**, *110*, 4365–4370.
(33) Ernst, K. H. *Interface Science* **2008**, *13*, 54–59.
(34) Cardona, C. M.; Li, W.; Kaifer, A. E.; Stockdale, D.; Bazan, G. C. *Adv. Mater.* **2011**10.1002/adma.201004554.
(35) Heinze, J.; Frontana-Uribe, B. A.; Ludwigs, S. *Chem. Rev.* **2010**, *110*, 4724–4771.
(36) Casalbore-Miceli, G.; Camaioni, N.; Geri, A.; Ridolfi, G.; Zanelli, A.; Gallazzi, M. C.; Maggini, M.; Benincori, T. *J. Electroanal. Chem.* **2007**, *603*, 227–234.
(37) Berger, R.; Butt, H. J.; Retschke, M. B.; Weber, S. A. L. *Macromol. Rapid Commun.* **2009**, *30*, 1167–1178.
(38) Kline, R. J.; McGehee, M. D. *Polymer Rev.* **2006**, *46*, 27–45.
(39) Facchetti, A.; Letizia, J.; Yoon, M.-H.; Mushrush, M.; Katz, H. E.; Marks, T. J. *Chem. Mater.* **2004**, *16*, 4715–4727.
(40) Naber, R. C. G; Tanase, C.; Blom, P. W. M.; Gelinck, G. H.; Marsman, A. W.; Touwslager, F. J.; Setayesh, S.; De Leeuw, D. M. *Nature Mat.* **2005**, *4*, 243–248.
(41) Lehn, J. M. *Rep. Prog. Phys.* **2004**, *67*, 249–265.